Fuel Processing Technology 137 (2015) 139-147
http://dx.doi.org/10.1016/j.fuproc.2015.04.016

Activated carbons from waste biomass and low rank coals as catalyst supports for hydrogen production by methanol decomposition

B. Tsyntsarski[1]*, I. Stoycheva[1], T. Tsoncheva[1], I. Genova[1], M. Dimitrov[1], B. Petrova[1], D. Paneva[2], Z. Cherkezova-Zheleva[2], T. Budinova[1], H. Kolev[2], A. Gomis-Berenguer[3], C.O. Ania[3], I. Mitov[2], N. Petrov[1]

[1]*Institute of Organic Chemistry with Centre of Phytochemistry, Bulgarian Academy of Sciences, Acad. G. Bonchev str., BL.9, 1113 Sofia, Bulgaria*

[2]*Institute of Catalysis, Bulgarian Academy of Sciences, Acad. G. Bonchev str., BL.11, 1113 Sofia, Bulgaria*

[3]*Instituto Nacional del Carbon (INCAR, CSIC), Apdo. 73, 33080 Oviedo, Spain*

Abstract

Activated carbons with different textural and chemical surface characteristics were synthesized from waste biomass and low rank coals, and furthermore used as a host matrix for cobalt species, varying the preparation and modification methods. The obtained activated carbons and modified samples were characterized by complex of various physicochemical methods, such as: low temperature physisorption of nitrogen, XRD, EPR, XPS, UV-Vis and TPR with hydrogen. Boehm method was applied for qualitative and quantitative determination of oxygen-containing groups on the carbon surface before and after cobalt deposition. The catalytic properties of cobalt modifications were tested in methanol decomposition. The dominant effect of activated carbon texture over the surface chemistry on the state and catalytic behaviour of cobalt species was discussed.

Keywords: activated carbon; waste biomass; coal tar pitch; cobalt modification; methanol decomposition; hydrogen.

* Corresponding author.
Tel: +359 29606-145. E-mail address: boyko.tsyntsarski@abv.bg (B. Tsyntsarski)

1. Introduction

As a catalyst support, activated carbon has many advantages, such as high surface area, tunable pore structure and surface chemistry, resistance to acidic or basic media, stability at high temperatures in inert or reduction atmosphere, as well as ability to recover the supported active metals [1, 2]. Activated carbons structure is developed by imperfect aromatic sheets of carbon atoms, as well as incompletely saturated valences and unpaired electrons on the surface. This determines high adsorption capacity of carbon materials, especially towards polar or polarizable molecules [3].

The surface functional groups, formed as a result of thermal or chemical treatments, influence the acid-base properties of carbon surface and could be considered as potential active sites for adsorption and catalysis [4, 5].

Carbon precursor selection and treatment conditions are feasible way for tuning the surface chemistry of carbon materials. On the other hand, porous structure of activated carbon is an important factor for preparation of efficient carbon-supported catalysts and it could be successfully regulated by the method of carbon synthesis and subsequent activation. It is well known, that the synthesis of porous carbon materials from lignocellulose precursors using conventional physical and chemical activation is the most economical and easy approach for large-scale production [5]. Thus synthesized activated carbons exhibit well-developed, however predominantly microporous structure [6, 7]. Previous studies report the benefits of addition of metal species (such as calcium) which increases the amount of volatile products during the pyrolysis process, and thus provides formation of carbon products with much broader pore size distribution (development of meso- and macroporosity) [8].

Supported cobalt materials have been investigated in a range of catalytic reactions including Fischer–Tropsch synthesis (FTS) [9, 10], methane [11, 12] and propane combustion [13], cyclohexane [14], ethyl acetate [15], cyclohexanol [16] and CO oxidation [17], etc. It was

demonstrated that the chemical nature of the support [18, 20], the texture and surface acidity [15, 19, 20], the composition of the metal precursor, the modification method and the intended metal loading influence the dispersion, reduction and catalytic properties, and the extent of metal–support interactions [15]. Various supports have been used for preparation of cobalt based catalysts, such as SiO_2, Al_2O_3, MgO, TiO_2, Nb_2O_5, CeO_2, and ZrO_2, but in some cases, formation of solid solutions between cobalt phase and support significantly changed the coordination and catalytic properties of cobalt [21, 22, 23]. The effect of carbon support on the formation of complex mixture of cobalt species in different oxidative state was discussed [24].

There are a lot of reports for the application of activated carbon supported cobalt catalysts for NOx reduction [22, 23, 25 - 31], oxidation of phenol with peroxymonosulphate [32], CO- PROX reaction [33], etc.

The aims of this paper are:

1) To obtain activated carbons with different surface and texture features from different precursors - waste agricultural products (peach stones, olive stones) and low rank coal treatment products, using various preparation technologies;

2) The synthesized activated carbons to be modified with cobalt and tested as catalysts in methanol decomposition. Recently methanol has been considered as a promising carrier of hydrogen due to methanol production by well developed technologies from waste biomass, and possibility for easy release of hydrogen if needed [34 - 37].

3) Finally, this investigation is focused on the possibility for fine tuning and improving catalyst behavior by tailoring the properties of carbon support, by varying the nature of the precursor and the preparation procedures. In this way, the scope of this study is related to the problem of hydrogen production and storage by utilization of waste biomass and coal treatment products.

2. Materials and methods

2.1 Synthesis of activated carbons

Olive stones based activated carbon, denoted as OSAC, was produced by one-step hydro-pyrolysis process, which is well studied and used for a long time in our laboratory [38 – 42]. Crushed olive stones are used as a precursor. Carbonization and subsequent activation procedures were performed in the presence of water vapor at 1023 K for 1 h. The flow of water vapor was started at 573 K.

Peach stones based activated carbon, denoted as PSAC, was produced by two-step process, including carbonization of crushed peach stones at 823 K for 1 h and subsequent activation of the carbonizate with water vapor at 1023 K for 1 h.

The synthetic activated carbon, denoted as SACS, was prepared by method, developed in our institute [42], using the following procedure: treatment of a mixture from coal tar pitch and furfural (1:1 by weight) with H_2SO_4 at 393 K until solidification. The solid product was subjected to further carbonization up to 873 K; the activation of the obtained carbonizate was performed at 1073 K in the presence of water vapor, followed by thermal treatment in Ar (99.996% purity, SIAD) atmosphere at 1473 K for 1 h.

The synthetic activated carbon, denoted SACN, was prepared from mixture from coal tar pitch and furfural (1:1 by weight) with HNO_3 at 393 K until solidification. The obtained solid product was subjected to further carbonization up to 873 K; the activation of the obtained carbonizate was performed at 1073 K in the presence of water vapor.

Ordered mesoporous silica of SBA-15 type (used as a reference support) was prepared according to the special synthesis procedure [43], using Pluronic 123 as a structure directing agent and decomposition of the template after heating at 823 K for 6 h in air.

2.2 Modification of activated carbons

The activated carbons and mesoporous silica were modified with Co by incipient wetness impregnation with aqueous solution of cobalt nitrate precursor. The nitrate decomposition was carried out by heating at 773 K for 6 h in a flow of nitrogen (99.96% purity, SIAD). The metal content in all samples is about 8 wt %, determined by atomic absorption spectroscopy. The cobalt modifications samples are denoted as Co/OSAC, Co/PSAC, Co/SACS and Co/SACN, respectively. The reference silica supported sample was denoted as Co/SBA-15.

2.3 Methods of characterization

The porous structure of all investigated activated carbons was studied by nitrogen adsorption at 77 K, carried out in an automatic Micromeritics ASAP 2010 volumetric apparatus. Before the experiments, the samples were outgassed under vacuum at 300 °C overnight.

The obtained isotherms were used to calculate the specific surface area S_{BET}, pore volumes and pore size distribution by using the method of density functional theory (DFT) [44].

The amount of various acidic oxygen-containing functional groups was determined by Boehm method using aqueous solutions of $NaHCO_3$, Na_2CO_3, NaOH, and C_2H_5ONa, according to the procedure described by Boehm [45]. The amount of basic sites was determined with 0.05 N HCl, according to the procedure described by Papirer et al. [46]. The pH of activated carbons was determined after boiling for 5 min in 100 cm^3 distilled water, followed by decantation and cooling down the solution to ambient temperature.

The electron paramagnetic resonance (EPR) measurements were performed by a X-band spectrometer Radiopan, working at 9.3 GHz and modulation 100 kHz. The measurements were taken with attenuation of 20 dB (about 0.7 mW) to avoid microwave saturation. The spectral data were processed by an on-line computer. In the EPR investigations ultramarine was used as a

reference for the determination of concentration of paramagnetic centers, and a ruby crystal, permanently placed in the spectrometer cavity, was the secondary reference.

Powder X-ray diffraction patterns were collected by a Bruker D8 Advance diffractometer with CuK_α radiation and LynxEye detector; the average crystallite size was evaluated according to Scherrer equation. The ultraviolet-visible light (UV–Vis) spectra were recorded using a Jasco V-650 UV-Vis spectrophotometer equipped with a diffuse reflectance unit. X-ray photoelectron spectra (XPS) measurements have been carried out on ESCALAB MkII (VG Scientific) electron spectrometer with pressure of $5x10^{-10}$ mbar in the analysis chamber, using twin anode MgK_α/AlK_α X-ray source with excitation energies of 1253.6 and 1486.6 eV, respectively. The spectra are recorded at total instrumental resolution (as it was measured with the FWHM of $Ag3d_{5/2}$ photoelectron line) of 1.06 eV and 1.18 eV, for MgK_α and AlK_α, respectively. Temperature-programmed reduction and thermo-gravimetric (TPR-TG) analysis was performed in a Setaram TG92 instrument in a flow of 50 vol% H_2 in Ar (100 cm^3 min^{-1}) and heating rate of 5 K min^{-1}.

2.4 Catalytic tests

Methanol decomposition was carried out in a fixed–bed reactor at atmospheric pressure. The catalyst (0.055 mg) with a particle size of 0.2-0.8 mm was diluted with three-fold higher amount (by volume) of glass spheres. The catalysts were tested under conditions of a temperature-programmed regime within the range of 350–770 K with a heating rate of 1 K min^{-1}.

Typically, the catalytic experiments includes: (i) catalyst pretreatment at 373 K in Ar for 1 h; (ii) GC analysis of the non-converted reaction mixture of methanol (1.57 kPa) in argon (50 ml/min); (iii) inserting the reaction mixture into the reactor at 350 K. After GC analysis of the output composition, the temperature in the reactor was increased with 20 K (1K/min). The last procedure was repeated every 20 K in the whole investigated temperature interval (350–770 K).

The changes in the catalysts during catalytic test were elucidated by in-situ measurements of the catalytic activity of the used catalysts at selected temperatures. During the experiments the reactant (methanol) as well as all carbon-containing products (CO, CO_2, methane, methyl formate and dimethyl ether) were in a gas phase and their amounts were determined by on-line GC analyses, using HP apparatus equipped with flame ionization and thermo-conductivity detectors, and a 30 m PLOT Q column. The methanol conversion *X(T)* at specific temperature *T* was calculated by the equation $X(T) = 100\% (C_{input}-C_{output})/C_{output}$, where C_{input} and C_{output} are the methanol concentrations in the gas mixture at the input and output of the reactor, respectively. The selectivity to CO, which formation was directly related to the production of hydrogen from methanol, was calculated by the equation $S_{CO} = 100\% \ Y_{CO}/X(T)$, where Y_{CO} was the yield of CO and *X(T)* was the conversion at selected temperature *T*.

3. Results and discussion

3.1 Activated carbons

3.1.1 Structure and texture characterization

Nitrogen adsorption isotherms of the obtained carbons are presented in Fig. 1a and the textural parameters are listed in Table 1. All isotherms are of hybrid I/IV type, according to the IUPAC classification [4], with a clear opening of the knee at low relative pressures. This indicates that all carbon materials have a complex microporous/mesoporous structure with domination of micropores. The highest BET surface area and pore volume with presence of extremely high amount of micropores are registered for OSAC (Table 1).

From all samples, SACN has the highest extent of developed mesoporosity, while the carbon treated at 1473 K (SACS) is characterized by the lowest BET surface area and pore volume.

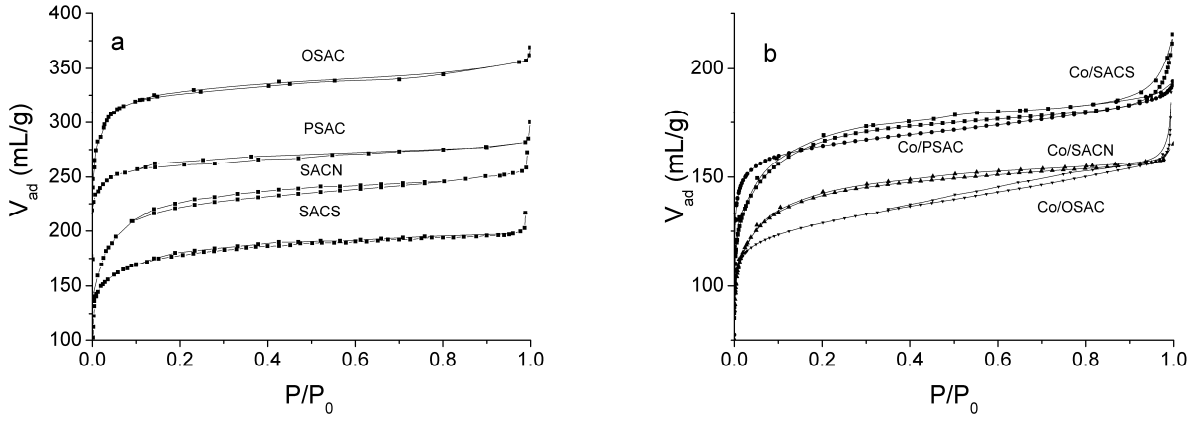

Figure 1. Nitrogen physisorption isotherms of the obtained activated carbons (a) and their cobalt modifications (b).

Table 1. Textural parameters of activated carbons and their cobalt modifications.

Sample	S_{BET}	ΔS_{BET}	V_{mic}[a]	V_{mes}[a]	$V_{mic}+V_{mes}$	$\Delta(V_{mic}+V_{mes})$	V_{mic}/V_{mes}
	m^2g^{-1}	%	$m^3.g^{-1}$	$m^3.g^{-1}$	$m^3.g^{-1}$	%	
OSAC	950		0.415	0.031	0.446		13.39
PSAC	830		0.345	0.054	0.399		6.39
SACS	680		0.215	0.030	0.245		7.17
SACN	820		0.301	0.104	0.405		2.89
Co/OSAC	604	36	0.235	0.039	0.274	38	6.03
Co/PSAC	617	26	0.241	0.042	0.283	29	5.74
Co/SACS	462	32	0.158	0.016	0.174	29	9.88
Co/SACN	556	32	0.196	0.022	0.218	46	8.91
SBA-15	807		0.120	0.860	0.980		0.14
Co/SBA-15	781	3	0.230	0.650	0.880	10	0.35

a - evaluated by DFT method.

Figure 2 shows X-ray diffraction (XRD) patterns of the activated carbons. The reflections around 23^o (002 plane) and 43^o (100 plane) are generally assigned to the formation of crystalline carbonaceous structure [47].

From the position of the (002) reflection, interplanar spacing d_{002} was calculated by application of Bragg's Law, while the average values of the crystallite height (L_c) and width (L_a) are obtained using Debye–Scherrer equation (Table 2).

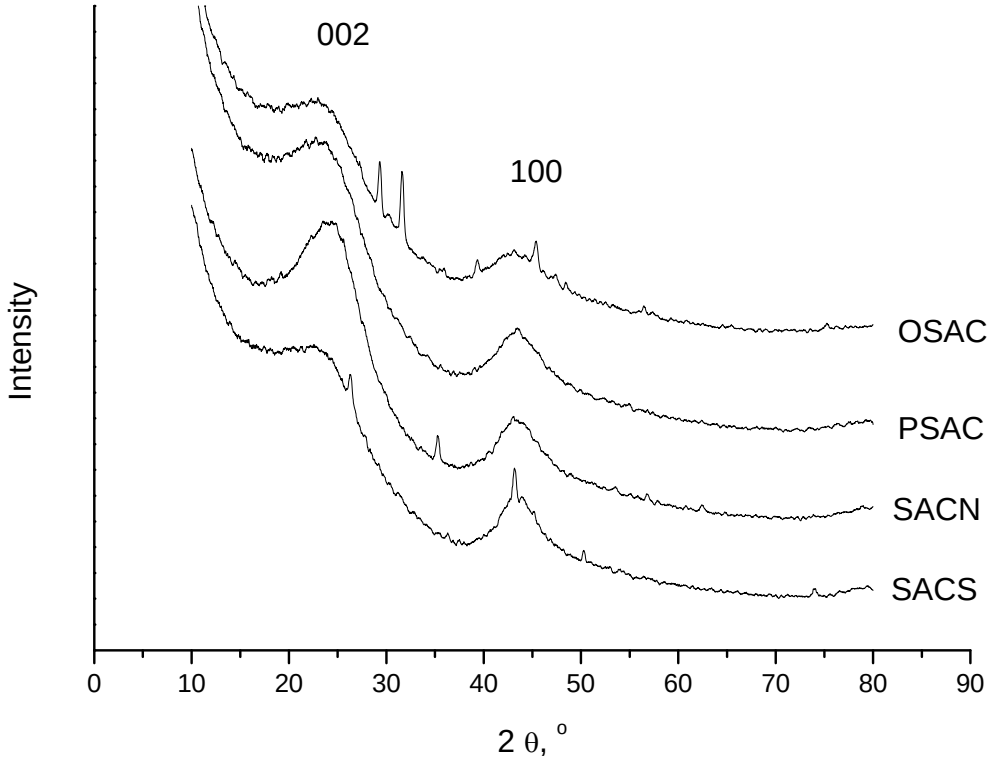

Figure 2. X-ray diffraction of the investigated activated carbons.

SACN sample have the lowest d_{002} and d_{100} distances and the highest value of L_c. This indicates higher degree of graphitization and more ordered and compact structure for SACN sample in comparison with the other carbons. Just the opposite, the highest d_{002} distance and the lowest value of L_c are established for SACS. This result seems to be quite surprising, taking into account the extremely high temperature treatment, which was applied during the preparation of this sample. It is

not excluded the observed effect to be provoked by the catalytic activity of H_2SO_4 in polycondensation reactions, which occur during thermo-oxidation treatment of the precursor. As a result, the formation of significant amount of crystallization centers, which hinders the arrangement of the aromatic layers, should be expected.

Table 2. XRD parameters for parent activated carbons.

X-ray parameters	Sample			
	OSAC	PSAC	SACS	SACN
2θ, degrees - Position 002	22.47	22.77	22.46	22.97
2θ, degrees - Position 100	43.10	43.38	43.21	43.48
d_{002}, nm (distance between C atoms of adjacent planes)	0.3957	0.3905	0.3959	0.3872
d_{100}, nm (distance between C atoms in the plane)	0.2098	0.2086	0.2094	0.2081
L_c, nm (002) average crystallite height FWHM	0.6559	0.6335	0.5587	0.7163
L_a, nm (100) average crystallite width FWHM	3.8242	2.1205	3.2256	2.7910

3.1.2 Chemical characterization

In Table 3 some chemical characteristics of the carbons are presented. All samples are characterized by low ash content (0.1-0.2 wt.% for the AC from coal tar pitch and 1.1-1.5 wt.% for the AC from biomass). Acidic (mainly carbonyl and hydroxyl) and basic groups are detected for OSAC, SACN, PSAC. The amount of surface acidic groups is below detection limit for SACS, obviously due to the high temperature treatment (which removes heteroatoms) during the preparation procedure.

Surprisingly, the titration with HCl reveals that the SACS sample is characterized with relatively high basicity. This fact can be hardly explained with the presence of basic groups on the carbon

surface, and in accordance with Petrova et al. [42], formation of surface OH groups, due to the interaction of π- sites from the carbon surface with adsorbed water molecules, could be proposed.

Table 3. Chemical characteristics of the obtained porous carbons.

Sample	Acidic groups, meq/g				Basic groups, meq/g	pH	Ash content wt. %
	Carboxylic	Lactonic	Hydroxyl	Carbonyl			
OSAC	0.02	0.09	0.55	1.07	1.03	9.2	1.15
PSAC	BDL[a]	BDL[a]	0.49	0.98	1.04	9.4	1.45
SACS	BDL[a]	BDL[a]	BDL[a]	BDL[a]	0.44	8.1	0.20
SACN	0.01	0.06	0.41	0.88	0.98	7.9	0.10
Co/OSAC	0.18	0.21	0.72	1.21	0.78	6.0	-
Co/PSAC	0.08	0.12	0.60	1.05	0.71	6.1	-
Co/SACS	0.02	0.05	0.24	0.79	0.68	6.8	-
Co/SACN	0.20	0.36	0.88	1.43	0.86	5.9	-

[a] BDL – below detection limit

3.1.3 EPR investigations

EPR analysis was performed for determination of the amount of unpaired electrons and the presence of heteroatoms [48 - 49] in the investigated carbons. These unpaired electrons are stabilized during carbonization process, due to bond cleavage at the edges of aromatic graphene sheets, thus forming edge carbon atoms, which can bind heteroatoms – O, N, etc. These carbon atoms are highly reactive centers, which determine the surface reactivity, surface reactions, and catalytic reactions of carbons. In principle the EPR spectrum of carbon materials represents characteristic singlet with different width and intensity. The EPR spectra and calculated data are shown in Figure 3 and Table 4. The studied carbons are characterized by different number of paramagnetic centers (PMC) and g-factor values. PMCs and heteroatoms are not detected for SACS. This confirms the assumption (see above section 3.1.2.) that the heat treatment up to 1473 K totally removes heteroatoms from the carbon, leading to formation of carbon atoms with completely hybridized bonding orbitals. The highest

amounts of PMCs and heteroatoms are detected in OSAC sample (Table 4). The high value of g-factor for this sample is in agreement with the data from the chemical analysis, which indicated the highest amount of surface functional groups (Table 3). In the same time, the SACN carbon has higher number of PMCs as compared to PSAC. These results accounts for considerable increase of the amount of surface oxygen groups for SACN in comparison with PSAC (Table 3), which could be due to the oxidation treatment with HNO_3 during the preparation procedure.

Table 4. EPR data for the investigated activated carbons.

Sample	g-factor	Area/Mn	Number of paramagnetic centers, x 10^{17}
SACS	0	0	0
PSAC	2.00234	2601.58	7.10
SACN	2.00225	6387.84	17.71
OSAC	2.00292	12910.04	35.80

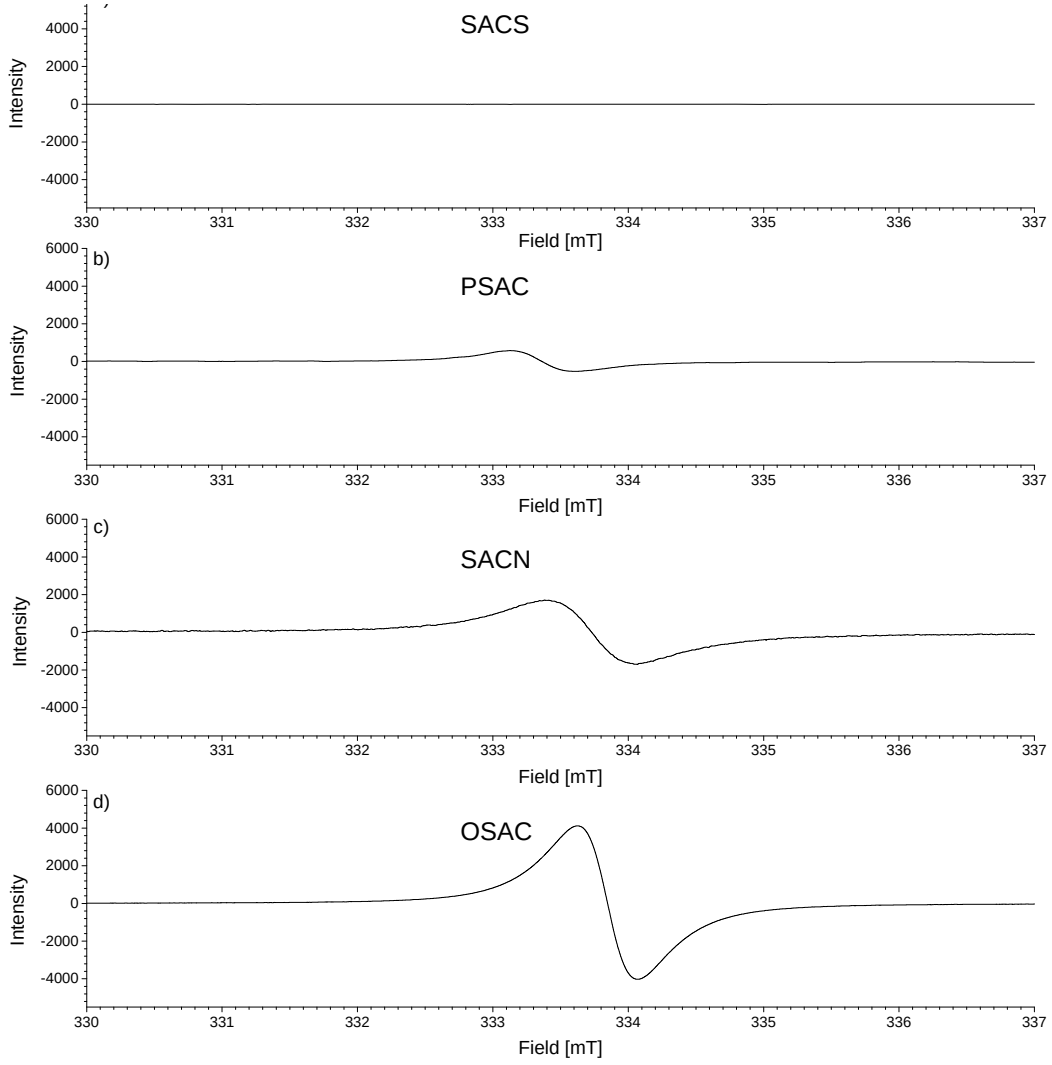

Figure 3. EPR spectra of activated carbons.

3.2 Cobalt modifications of activated carbons

3.2.1 Structural and chemical characterization

The nitrogen adsorption isotherms of cobalt modified carbons are presented in Fig.1b and the corresponding textural parameters are listed in Table 1. The decrease in the BET surface area and pore volume for all carbon samples after modification clearly indicates deposition of cobalt phase into the carbon porous structure. The observed significant decrease in the microporous volume with the preservation of mesopores for Co/OSAC indicates that there are cobalt particles located into the micropores of this carbon support.

Just the opposite, despite the observed decrease in the V_{mic} and V_{mes} for Co/SACN, the V_{mic}/V_{mes} ratio increases about 3 times which evidences predominant location of cobalt species into the mesopores of SACN. The decrease in the BET surface area and pore volume for Co/PSAC and Co/SACS is combined with slight changes in the V_{mic}/V_{mes} ratio, which could be related to almost random deposition of cobalt species into the micro- and mesopores for these carbon supports.

For comparison, the nitrogen adsorption analysis for the reference SBA-15 support show that it has BET surface area close to activated carbons, but with higher pore volume, developed mainly from ordered mesopores (Table 1). The modification of SBA-15 with cobalt leads to a significant decrease in the mesopore volume, probably due to deposition of cobalt species in the mesopores.

XRD patterns of activated carbon modifications are presented in Fig. 4. The modified carbon samples are characterized by formation of carbonaceous crystalline structure with reflexes at 24^o and 44^o. The low intensity reflections at 36.6 ^{o} and 42.4 ^{o} indicate presence of finely dispersed CoO (PDF 43-1004) particles with average crystalline size 18-20 nm. The appearance of small reflection at 44.4 ^{o} in the XRD patterns of Co/SACN and Co/OSAC is evidence of formation of small portion of metallic Co_{fcc} nanoparticles (PDF 15-0806) with average crystalline size 20-35 nm. XRD pattern of Co/SBA-15 (Fig. 4) represents broad and low intensive reflections at 36.6 ^{o}, 59.4 ^{o} and 65 ^{o}, typical for Co_3O_4 spinel oxide (PDF 3-1003) with average particles size about 15 nm.

The data from chemical analysis of carbon after cobalt modification are shown in Table 3. A well expressed effect of the formation of new portion of surface acidic groups as compared to the corresponding parent carbon supports is demonstrated. This observation is not surprising, taking into account the possibility for oxidation of carbon surface by the products (O_2 and NO_2) of cobalt nitrate decomposition during the thermal treatment. Despite the lower number of PMCs in SACN in comparison with OSAC (Table 4), the increase in the amount of oxygen groups in the former is more significant (Table 3). This could be due to the higher number of micropores in OSAC, which are inaccessible for NO_2 and O_2 molecules.

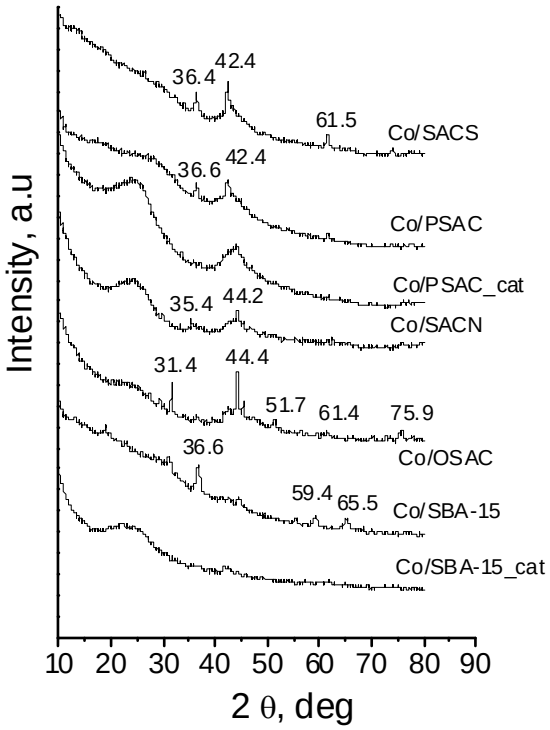

Figure 4. XRD patterns of cobalt modifications of activated carbons and reference SBA-15 sample. For selected samples XRD patterns after the catalytic test are presented (cat).

Obviously, both capillary and surface effects control the formation of cobalt phase on activated carbons. Contrary to the case of Co/SBA-15, the decomposition of cobalt nitrate precursor in inert atmosphere on carbon leads to the formation of reduced cobalt species (Co^0 and/or CoO), which evidences the specific effect of carbon surface on the formation of cobalt active phase.

Besides, metallic cobalt particles were observed only for Co/OSAC and Co/SACN. Taking into account XRD data (Fig. 2), chemical analysis (Table 3) and texture analysis (Table 1), we could assume that the higher reduction effect is due to the presence of considerably higher amount of PMCs, better packed structure, dominant presence of micro- and mesopores, and higher amount of oxygen functional groups on the surface of these carbons (OSAC and SACN), in comparison with other carbons.

3.2.2 XPS and UV-vis investigations of cobalt species

In order to obtain more information for the oxidation state of cobalt species, UV-Vis and XPS investigations were performed. The UV-Vis spectrum of reference Co/SBA-15 (Fig.5) contains a broad absorption band around 470 nm, which can be attributed to octahedrally coordinated Co^{3+} [15]. The band at around 720 nm is ascribed to the electronic ligand-field 4A2(F)→4T1(p) transition of Co^{2+} in tetrahedral coordination. Thus the UV-Vis study confirms the data from XRD analysis, indicating presence of Co_3O_4 phase in Co/SBA-15. The absorption peaks for all cobalt modifications are very complex and the typical bands for the Co_3O_4 phase cannot be distinguished. However the slight absorption features with a maximum at about 460-500 nm could be assigned to the presence of Co^{2+} ions in octahedral coordination [50]. This is in accordance with the XRD data, which demonstrates that CoO was detected for all carbon modifications (Fig. 4).

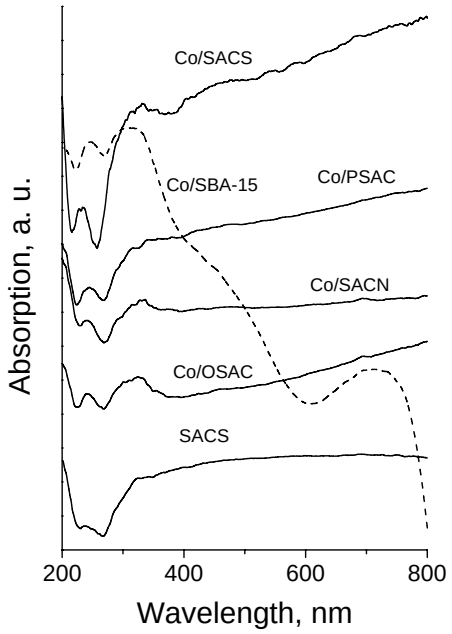

Figure 5. UV-Vis spectra of cobalt modifications of various AC. For comparison UV-Vis spectra of selected parent AC and Co/SBA-15 are also presented (dashed line).

XPS is a useful technique for investigation the surface element composition and oxidation state. The XPS spectra of selected samples are presented in Fig. 6. For all carbon based materials the $Co2p_{3/2}$ and $Co2p_{1/2}$ binding energies are 781.1-781.5 eV and 796.3-797.3 eV, respectively. The intensive satelite peaks at about 787 eV and 803 eV, and the spin-orbit splitting between 2p level peaks of about 15.8-16.0 eV, are consistent with the presence of Co oxide phase [14], which was also proved by XRD and UV-Vis analysis. For comparison, the $Co2p_{3/2}$ and $Co2p_{1/2}$ binding energies for Co/SBA-15 are 780.7 eV and 795.7 eV, respectively.

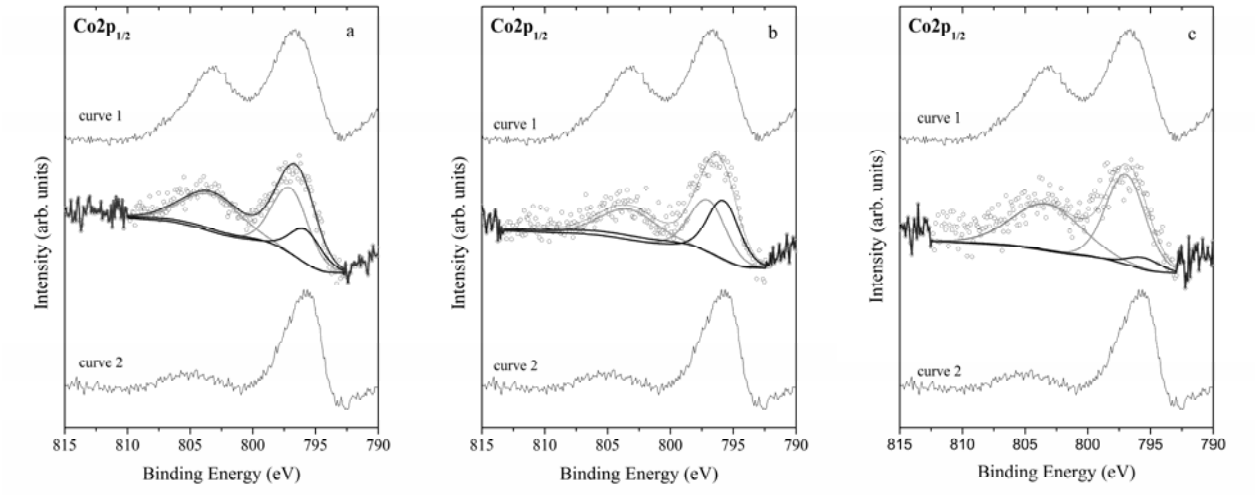

Figure 6. High resolution XP Co $2p_{1/2}$ spectra of Co/SACS (a), Co/PSAC (b) and Co/OSAC(c) compared with standard spectra of Co^{2+} (curve 1) and Co^{3+} (curve 2).

Very low satelite peaks are detected, which reveals predominantly presence of Co_3O_4 (also in accordance with XRD and UV-Vis measurements). In order to examine the cobalt oxidation state in details, curve fitting of $2p_{1/2}$ level was performed. Simulating the standard spectra of $Co2p_{1/2}$ for Co^{3+} and Co^{2+}, the curve fitting of high resolution XPS spectra to Co^{2+} and Co^{3+}constituents was performed (Fig.6) and their atomic concentrations are presented in Table 5. The binding energies of

the main peak, satellite position and the ratio between main peak area and satellite peak area are used for deconvolution of Co peaks. Thus, the line shape is included in the curve fitting. Although FWHM was not fixed during deconvolution, it is taken into account for the curve fitting shown in Fig.6. The curve fitting is based on the standard spectra for Co^{2+} and Co^{3+} (Fig.6, curves 1 and 2, respectively). The line shape of the curves indicate presence of Co^{3+} and Co^{2+} in different ratio with domination of Co^{2+} for Co/SACN and Co/OSAC (Table 5). This result is in agreement with the data from the XRD analysis, indicating that cobalt with higher degree of oxidation was detected. The surface atomic concentrations for the studied materials are presented in Table 5.

For almost all activated carbon modifications, the surface concentration of Co (2-3 at.%) is close to the bulk concentration, which indicates almost uniform distribution of cobalt phase in the sample. Only for Co/OSAC the surface concentration of Co is about twice higher than this expected for the bulk material. Taking into acount the nitrogen adsorption data, it could be concluded that this is due to the higher dispersion of cobalt phase after cobalt deposition in carbon micropores. Note the extremely low surface Co concentration for Co/SBA-15 (bellow 0.5 at.%), which may be attributed to the location of cobalt species deeply into the long mesopores of the silica matrix.

Table 5. Surface atomic concentrations (at. %) of presented elements. Co^{2+} and Co^{3+} atomic percentage are obtained by the curve fitting procedure of Co $2p_{1/2}$ peak.

Sample	C 1s	O 1s	Co $2p_{1/2}$		Si 2p	Na 1s	Cl 2p
			Co^{2+}	Co^{3+}			
Co/SACS	89	9	1.5	0.5			
Co/PSAC	90	8	1.1	0.9	-	-	-
Co/SBA-15	20	51	~0.3	~0.1	29	-	-
Co/SACN	87	8	2	0	3	-	-
Co/OSAC	77	13	3	~0.2	-	5	2

3.2.3 Temperature-programmed reduction

TPR is a powerful method to study the reduction behavior of oxidized phases, and in some cases - their dispersion and interaction with the support. Temperature-programmed reduction with thermo-gravimetric and differential thermo-gravimetric (TPR-TG and TPR-DTG) profiles of all carbon modifications are presented in Fig.7. The reduction profile of Co/SBA-15 (reference material) contains two main effects with a maximum around 564 K and 730 K, with about 1:3 weight-to-loss ratio. According to the XRD, UV-Vis and XPS data, this could be due to stepwise reduction of Co_3O_4 to metallic cobalt.

Note that the reduction degree in the whole temperature interval is about 50 %. In accordance with the XPS data, this could be due to the presence of less accessible cobalt oxide species, located deeply into the mesopores of silica support. The existence of strong interaction between the finely dispersed cobalt species and surface silanol groups which suppresses their reduction is not excluded [51]. The TPR profiles of all carbon supported materials differ significantly from the TPR profile of Co/SBA-15.

For the carbon supported samples: (i) the reduction process starts at about 50-100 K lower temperature; (ii) depending on the carbon used one or several reduction effects in the low temperature region (400-600 K) are detected; (iii) the observed weight loss in the low temperature region is about 3-4 times higher than this for the Co/SBA-15 analogue, but it is lower than the calculated one for the reduction of CoO to metallic cobalt; (iv) extremely high TPR effect above 650 K is detected.

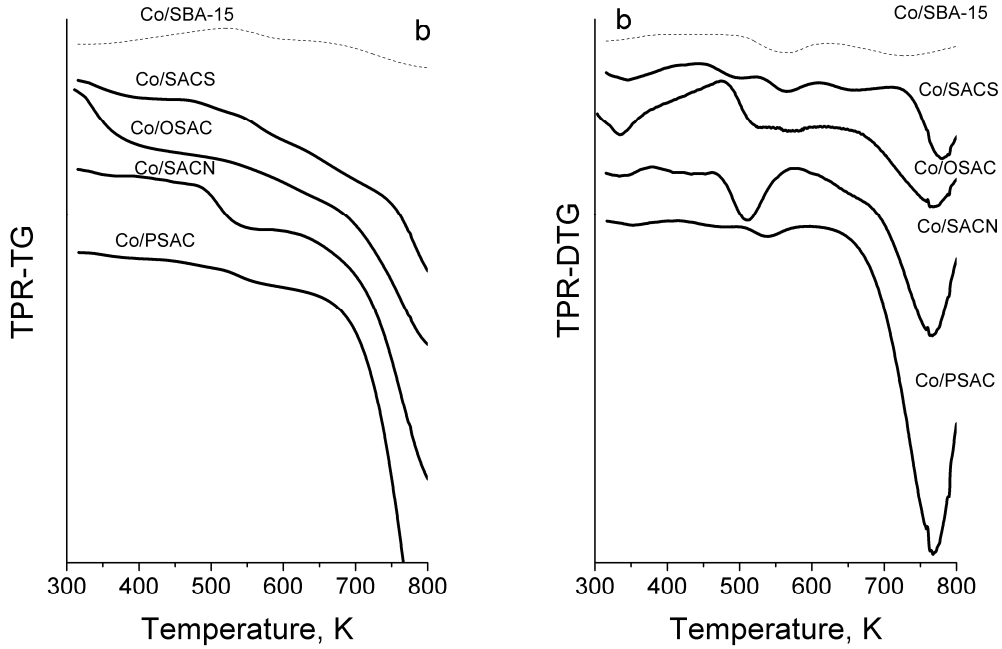

Figure 7. TPR-TG (a) and TPR-DTG (b) profiles for cobalt modifications of various activated carbons (the curves are shifted along the y axis). For comparison, TPR-TG and TPR-DTG profiles of SBA-15 is also illustrated (dashed lines).

These observations evidence formation of more complex and easily reducible cobalt phase on the activated carbon support as compared to the SBA-15 silica.

Coexistence of metallic cobalt and CoO_x species in different state and proportion [52] depending on the nature of the activated carbon support is assumed. The presence of cobalt species on AC provokes the release of volatile products under reduction conditions above 650 K. This effect is less pronounced for SACS and OSAC, and the highest for PSAC. This assumption is consistent with the conception of Rodrigues-Reinoso [1] and should be taken into consideration during the estimation of catalyst stability under the reduction reaction medium.

3.2.4 Catalytic tests

Fig. 8a shows temperature dependence of methanol decomposition on various cobalt modifications. CO is detected as main carbon-containing product and selectivity towards CO is shown in Fig. 8b.

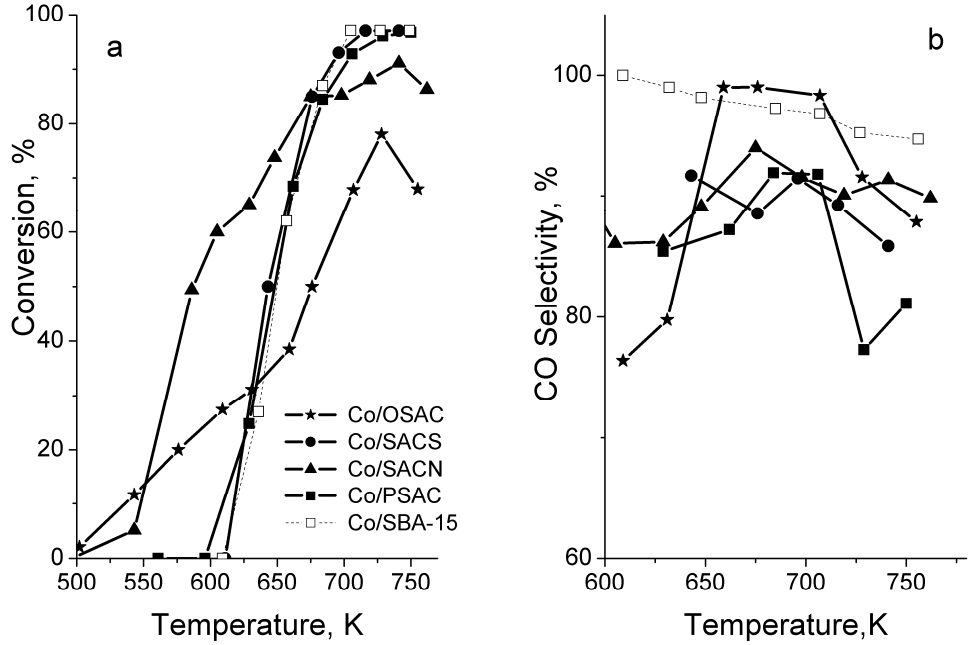

Figure 8. Methanol conversion (a) and CO selectivity (b) vs temperature for various cobalt modifications.

CH_4 and CO_2 are also registered as by-products. The conversion curve for Co/SACN is about 100 K shifted to lower temperature as compared to the other catalysts, clearly indicating the highest activity in methanol decomposition, combined with about 90% selectivity to CO.

Co/OSAC also demonstrates catalytic activity in the same low temperature region, but it is relatively lower than Co/SACN. Both carbons are distinguished with considerably higher amount of PMCs and oxygen functionalities. This fact indicates the important role of these characteristics for the catalytic activity of the samples. The presence of surface oxygen-containing groups on activated carbon (Table 3 and Table 4) seems to facilitate the formation of highly dispersed and partially reduced (to metallic Co) active phase (Fig. 4), which decompose methanol at relatively low temperatures. However, the location of cobalt phase into mesopores reveals formation of more uniform and accessible to reactants cobalt species (Table 1, Fig.4), which provides higher catalytic activity for Co/SACN. Just the opposite, the predominant location of cobalt species into micropores of OSAC hinders their participation in the catalytic process. This is well illustrated not only with

the smoother profile of the conversion curve for this sample but also with the appearance of maximum in it. The conversion curves for Co/PSAC and Co/SACS are similar. They are much steeper and shifted to higher temperatures as compared to other two modifications. Obviously, the predominant presence of cobalt oxide phase, randomly distributed into micro- and mesopores of these carbon supports, facilitate the catalytic activity and stability, but at relatively higher temperatures. Taking into account the physicochemical characteristics of these samples, it can be assumed, that surface functionalities of activated carbons do not have dominant effect on the formation of cobalt phase and its catalytic activity, however the crucial role of texture characteristics of carbon supports is demonstrated.

For comparison, Co/SBA-15 has lower catalytic activity, but higher stability and selectivity to CO, in comparison with Co/SACN. According to physicochemical analysis, this catalytic behaviour is assigned to the formation of Co_3O_4 spinel species (Figs. 4-6), which are located deeply into the mesopores and are in strong interaction with surface silanol groups.

Additional catalytic tests with used activated carbon based materials after catalytic process clearly demonstrate a decrease in the catalytic activity. This decrease is about 3 and 6 times, for Co/SACN and Co/OSAC, respectively, and it is much lower for Co/SACS and Co/PSAC. Just the opposite, no significant changes with the catalytic activity are registered for the used Co/SBA-15. The XRD patterns of the used catalysts confirm reduction changes with the formation of metallic Co for the AC supported materials and disappearance of crystal Co_3O_4 phase (Fig.4) with the formation of finely dispersed CoO species for the SBA-15 analogue (Fig.4).

4. Conclusions

The synthetic activated carbon (SACN), prepared by thermo-chemical treatment of a mixture of coal tar pitch and furfural with HNO_3, is characterized by relatively high amount of mesopores, which facilitate the deposition of uniform, accessible and highly active in methanol decomposition

cobalt species. Similar preparation procedure, but in the presence of H_2SO_4, leads to formation of highly disordered carbon structure. The treatment of this material above 1447 K (SACS) fully releases the surface functional groups and favors formation of highly dispersed and relatively highly active cobalt particles The activated carbon, prepared by two-step carbonization-activation procedure from peach stones (PSAC), after further modification with cobalt, exhibits low thermal stability in reduction atmosphere above 700 K. The activated carbon, obtained by one-step carbonization-activation procedure from olive stones (OSAC), demonstrates extremely high amount of surface functional groups and predominantly microporous structure, which promotes the formation of highly dispersed cobalt species, located mainly into the micropores.

This makes them less accessible for the reactant molecules and as a result decreases their catalytic activity. Despite the important role of carbon paramagnetic centers and oxygen functionalities on the catalytic activity of cobalt modifications, especially at low temperature, the dominant effect of carbon texture over the surface functionalities is considered.

Acknowledgements

Financial support from Bulgarian Academy of Sciences and Bulgarian Ministry of Education (Projects DFNI-E01/7/2012 and DFNI-E02/2/2014) is gratefully acknowledged.

References

[1] F. Rodriguez-Reinoso, The role of carbon materials in heterogeneous catalysis, Carbon 36 (1998) 159-175.
[2] H. Juntgen, Activated carbon as catalyst support, Fuel 65 (1986) 1436-1446.
[3] R.C. Bansal, J.B. Donnet, H.F. Stoeckli, Active Carbon, New York, Marcel Dekker, 1988.
[4] C. Moreno-Castilla, F. Carrasco-Marin, C. Parejo-Perez, M.V. Lopez Ramon, Dehydration of methanol to dimethyl ether catalyzed by oxidized activated carbon with varying surface acidic character, Carbon 39 (2001) 869-875.
[5] F. Rodriguez-Reinoso, M. Molina-Sabio, M.A. Munecas, Effect of microporosity and oxygen surface groups of activated carbon in the adsorption of molecules of different polarity, J. Phys. Chem. 96 (1992) 2707-2713.
[6] H. Marsh, F. Rodríguez-Reinoso, Activated Carbon, London, Elsevier; 2006.

[7] M. Molina-Sabio, M.T. González, F. Rodríguez-Reinoso, A. Sepúlveda-Escribano, Effect of steam and carbon dioxide activation in the micropore size distribution of activated carbon, Carbon 34 (1996) 505-510.
[8] J.M. Juárez-Galán, A. Silvestre-Albero, J. Silvestre-Albero, F. Rodríguez-Reinoso, Synthesis of activated carbon with highly developed mesoporosity, Micropor. Mesopor. Mater. 117 (2009) 519-521.
[9] H. Xiong, Y. Zhang, K. Liew, J. Li, Ruthenium promotion of Co/SBA-15 catalysts with high cobalt loading for Fischer–Tropsch synthesis, Fuel Proc. Technol. 90 (2009) 237-246.
[10] A. Martinez, C. Lopez, F. Marquez, I. Diaz, Fischer–Tropsch synthesis of hydrocarbons over mesoporous Co/SBA-15 catalysts: the influence of metal loading, cobalt precursor, and promoters , J. Catal. 220 (2003) 486-499.
[11] G. Laugel, J. Arichi, P. Bernhardt, M. Moliere, A. Kiennemann, F. Garin, B. Louis, Preparation and characterisation of metal oxides supported on SBA-15 as methane combustion catalysts, Comtes Rendus Chimie 12 (2009) 731-739.
[12] G. Laugel, J. Arichi, H. Guerba, M. Moliere, A. Kiennemann, F. Garin, B. Louis, Co_3O_4 and Mn_3O_4 Nanoparticles Dispersed on SBA-15: Efficient Catalysts for Methane Combustion, Catal. Lett. 125 (2008) 14-21.
[13] I. Yuranov, L. Kiwi-Minsker, A. Renken, Structured combustion catalysts based on sintered metal fibre filters, Appl. Catal. B: Environmental, 43 (2003) 217-227.
[14]. L. Zhou, J. Xu, H. Miao, F. Wang, X. Li, Catalytic oxidation of cyclohexane to cyclohexanol and cyclohexanone over Co_3O_4 nanocrystals with molecular oxygen, Appl. Catal. A: General 292 (2005) 223-228.
[15] T. Tsoncheva, L. Ivanova, J. Rosenholm, M. Linden, Cobalt oxide species supported on SBA-15, KIT-5 and KIT-6 mesoporous silicas for ethyl acetate total oxidation, Appl. Catal. B: Environmental 89 (2009) 365-374.
[16] J. Taghavimoghaddam, G.P. Knowles, A.L. Chaffee, Preparation and characterization of mesoporous silica supported cobalt oxide as a catalyst for the oxidation of cyclohexanol, J. Mol. Catal. A: Chemical 358 (2012) 79-88.
[17] I. Lopes, A. Davidson, C. Thomas, Calibrated Co_3O_4 nanoparticles patterned in SBA-15 silicas: Accessibility and activity for CO oxidation, Catal. Commun. 8 (2007) 2105-2109.
[18] T. Vralstad, G. Oye, M. Ronning, W.R. Glomm, M. Stocker, J. Sjoblom, Interfacial chemistry of cobalt (II) during sol–gel synthesis of cobalt-containing mesoporous materials, Micropor. Mesopor. Mater. 80 (2005) 291-300.
[19] A.Y. Khodakov, R. Bechara, A. Griboval-Constant, Fischer–Tropsch synthesis over silica supported cobalt catalysts: mesoporous structure versus cobalt surface density, Appl. Catal. A: General 254 (2003) 273-288.
[20] O. Gonzalez, H. Perez, P. Navarro, L.C. Almeida, J.G. Pacheco, M. Montes, Use of different mesostructured materials based on silica as cobalt supports for the Fischer–Tropsch synthesis, Catal. Today 148 (2009) 140-147.
[21] T. Das, G. Deo, Effects of metal loading and support for supported cobalt catalyst, Catal. Today 198 (2012) 116-124.
[22] B. Djonev, B. Tsyntsarski, D. Klissurski, K. Hadjiivanov, IR Spectroscopic Study of NO_x Adsorption and NO_x -O_2 Coadsorption on Co^{2+}/SiO_2 Catalysts, J. Chem. Soc., Faraday Trans., 93 (1997) 4055-4063.
[23] B. Tsyntsarski, V. Avreyska, Ts. Marinova, D. Klissurski, K. Hadjiivanov, FT-IR study of the nature and reactivity of surface NO_x compounds formed after NO adsorption and NO + O_2 coadsorption on zirconia- and sulfated zirconia-supported cobalt, J. Mol. Catal. A: Chemical 193 (2003) 139-149.

[24] J. Lu, Ch. Huang, S. Bai, Y. Jiang, Zh. Li, Thermal decomposition and cobalt species transformation of carbon nanotubes supported cobalt catalyst for Fischer-Tropsch synthesis, J. Natural Gas Chem. 21 (2012) 37-42.
[25] K. Hadjiivanov, B. Tsyntsarski, T. Nikolova, Stability and Reactivity of the Nitrogen-oxo Species formed after NO Adsorption and NO + O_2 Coadsorption on a Co–ZSM-5 deNO_x Catalyst. An FTIR Spectroscopic Study, Phys. Chem. Chem. Phys. 1 (1999) 4521-4528.
[26] F. Zhang, S. Zhang, N. Guan, E. Schreier, M. Richter, R. Eckelt, R. Fricke, NO SCR with propane and propene on Co-based alumina catalysts prepared by co-precipitation, Appl. Catal. B: Environmental 73 (2007) 209-219.
[27] T. Montanari, O. Marie, M. Daturi, G. Busca, Searching for the active sites of Co-H-MFI catalyst for the selective catalytic reduction of NO by methane: A FT-IR in situ and operando study, Appl. Catal. B: Environmental 71 (2007) 216-222.
[28] D. Pietrogiacomi, M.C. Campa, V. Indovina, FTIR of adsorbed species on Co-H-MOR and Co-Na-MOR under CH4 + NO + O2 stream: Catalytic activity and selectivity, Catal. Today 155 (2010) 192-198.
[29] X. Chen, A. Zhu, C.T. Au, X. Yang., C. Shi, The role of active sites of CoH-ZSM-5 catalysts for the C2H4-SCR of NO, Catal. Lett. 135 (2010) 182-189.
[30] Z.H. Zhu, L.R. Radovic, G.Q. Lu, Effects of acid treatments of carbon on N_2O and NO reduction by carbon-supported copper catalysts, Carbon 38 (2000) 451-464.
[31] Y.H. Hu, E. Ruckenstein, The Catalytic Reaction of NO over Cu Supported on Meso-Carbon Microbeads of Ultrahigh Surface Area, J. Catal. 172 (1997) 110-117.
[32] P.R. Shukla, S. Wang, H. Sun, H.M. Ang, M. Tade, Activated carbon supported cobalt catalysts for advanced oxidation of organic contaminants in aqueous solution, Appl. Catal. B: Environmental 100 (2010) 529-534.
[33] T. Bao, Z. Zhao, Y. Dai, X. Lin, R. Jin, G. Wang, T. Muhammad, Supported Co_3O_4-CeO_2 catalysts on modified activated carbon for CO preferential oxidation in H_2-rich gases, Appl. Catal. B: Environmental 119-120 (2012) 62-73.
[34] M. Zhao, X. Li, L. Zhang, C. Zhang, M. Gong, Y. Chen, Catalytic decomposition of methanol to carbon monoxide and hydrogen over palladium supported on $Ce_{0.65}Zr_{0.30}La_{0.05}O_2$ and La–Al_2O_3, Catal. Today 175 (2011) 430-434.
[35] J. Vancoillie, J. Demuynck, L. Sileghem, M. Van De Ginste, S. Verhelst, Comparison of the renewable transportation fuels, hydrogen and methanol formed from hydrogen, with gasoline – Engine efficiency study, Int. J. Hydrogen Energy 37 (2012) 9914-9924.
[36] Y. Lu, W. Yan, Sh. Hu, B. Wang, Hydrogen production by methanol decomposition using gliding arc gas discharge, J. Fuel. Chem. Technol. 40 (2012) 698-706.
[37] M. Cimenti, J.M. Hill, Importance of pyrolysis and catalytic decomposition for the direct utilization of methanol in solid oxide fuel cells, J. Power Sources 195 (2010) 54-61.
[38] K. Gergova, N. Petrov, S. Eser, Adsorption properties and microstructure of activated carbons produced from agricultural by-products by steam pyrolysis, Carbon 32 (1994) 693-702.
[39] N. Petrov, K. Gergova, S. Esser, Effect of water vapor on the porous structure of activated carbon from lignite, Fuel 73 (1994) 1197-1201.
[40] D. Savova, E. Apak, E. Ekinci, M. Ferhat Yardim, N. Petrov, Biomass conversion to carbon adsorbents and gas, Biomass and Bioenergy 21 (2001) 133-142.
[41] N. Petrov, T. Budinova, M. Razvigorova, J.-B. Parra, P. Galiatsatou, Conversion of olive wastes to volatiles and carbon adsorbents, Biomass and Bioenergy 32 (2008) 1303-1310.
[42] B. Petrova, B. Tsyntsarski, T. Budinova, N. Petrov, C.O. Ania, J.-B. Parra, M. Mladenov, P. Tzvetkov, Synthesis of nanoporous carbons from mixtures of coal tar pitch and furfural and their application as electrode materials, Fuel Proc. Technol. 91 (2010) 1710-1716.

[43] M. Choi, W. Heo, F. Kleitz, R. Ryoo, Facile synthesis of high quality mesoporous SBA-15 with enhanced control of the porous network connectivity and wall thickness, Chem. Commun. 12 (2003) 1340-1341.
[44] J. Olivier, Improving the models used for calculating the size distribution of micropore volume of activated carbons from adsorption data, Carbon 36 (1998)1469-1472.
[45] H.P. Boehm, Chemical Identification of Surface Groups, Adv. Catal. 16 (1966) 179-274.
[46] E. Papirer, S. Li, J.-B. Donnet, Contribution to the study of basic surface groups on carbons, Carbon 25 (1987) 243-247.
[47] C.A. Leon y Leon, J.M. Solar, V. Calemma, L.R. Radovic, Evidence for the protonation of basal plane sites on carbon, Carbon 30 (1992) 797-811.
[48] I. Tarkovskaja, Okislenii ugol, Kiev, Naukova dumka; 1981.
[49] D.I. Ingram, Free radicals as studied by electron spin resonance, London, Butterworths Scientific; 1958.
[50] L. Bai, F. Wyrwalski, J.-F. Lamonier, A.Y. Khodakov, E. Monflier, A. Ponchel, Effects of β-cyclodextrin introduction to zirconia supported-cobalt oxide catalysts: From molecule-ion associations to complete oxidation of formaldehyde, Appl. Catal. B: Environmental, 138-139 (2013) 381-390.
[51] F. Boubekr, A. Davidson, S. Casale, P. Massiani, Ex-nitrate Co/SBA-15 catalysts prepared with calibrated silica grains: Information given by TPR, TEM, SAXS and WAXS, Micropor. Mesopor. Mater. 141 (2011) 157-166.
[52] J.A. Diaz, M. Martinez-Fernandez, A. Romero, J.L. Valverde, Synthesis of carbon nanofibers supported cobalt catalysts for Fischer–Tropsch process, Fuel 111 (2013) 422-429.